Dynamical Spectral Function of the Kagome Quantum Spin Liquid

Jiahang Hu,[1,2,*] Runze Chi,[1,2,3,*] Yibin Guo,[1,2] B. Normand,[4,†] Hai-Jun Liao,[1,‡] and T. Xiang[1,2,§]
[1]*Beijing National Laboratory for Condensed Matter Physics and Institute of Physics, Chinese Academy of Sciences, Beijing 100190, China*
[2]*School of Physical Sciences, University of Chinese Academy of Sciences, Beijing 100049, China*
[3]*Division of Chemistry and Chemical Engineering, California Institute of Technology, Pasadena, California 91125, USA*
[4]*PSI Center for Scientific Computing, Theory and Data, Paul Scherrer Institute, CH-5232 Villigen-PSI, Switzerland*

(Received 23 December 2025; revised 27 March 2026; accepted 9 July 2026; published 14 August 2026)

Quantum spin liquids (QSLs) host exotic fractionalized magnetic and gauge-field excitations whose microscopic origins and experimental verification remain frustratingly elusive. In the absence of static magnetic order, the spin excitation spectrum constitutes the crucial probe of QSL behavior, but its theoretical computation is a serious challenge. Here we employ state-of-the-art tensor-network methods to obtain the full dynamical spectral function of the J_1-J_2 kagome Heisenberg model and benchmark our results by tracking their evolution across the magnetically ordered and QSL phases. Reducing $|J_2|/J_1$ causes increasingly strong spin-wave renormalization, flattening these modes then merging them into a continuum characteristic of deconfined spinons at all finite energies in the QSL. The low-energy continuum and the occurrence of gap closure at multiple high-symmetry points identify this gapless QSL as the U(1) Dirac spin liquid. These results establish a unified understanding of spin excitations in highly frustrated quantum magnets and provide clear spectral fingerprints for experimental detection in candidate kagome QSL materials.

DOI: 10.1103/fjjf-xspp

Introduction—Quantum spin liquids (QSLs) continue to attract extensive interest due to their unconventional properties, which are characterized by long-ranged quantum entanglement rather than conventional magnetic order at zero temperature, with accompanying fractional spin excitations [1–3]. QSLs offer exciting prospects for deepening our understanding of strongly correlated electronic systems, entanglement, topological order, and even error-protected quantum computation. The kagome lattice, with its frustrated triangular geometry and low coordination number, has long been a focal point for exploring the exotic states of quantum matter, and the $S = 1/2$ kagome model with only nearest-neighbor antiferromagnetic Heisenberg interactions is now widely accepted as hosting a QSL ground state.

This model presents one of the hardest problems in quantum magnetism [2,4–8] due to its extensive manifold of low-lying energy states. Introducing a next-neighbor coupling (J_2) is one of the more revealing ways to lower the degeneracy of this manifold and hence to track the emergence of QSL behavior [9–14]. Nevertheless, an accurate characterization of the spin dynamics remains a fundamental challenge. Every numerical method faces significant limitations in this problem due to the complex interplay of quantum fluctuations, frustration, and finite system sizes; although computational studies have provided valuable insight into the ground-state properties, a quantitative description of the spectral function at all energies has not been possible. This is particularly important because the excitation spectrum can be measured directly by techniques including inelastic neutron scattering (INS) and tunneling spectroscopy, making it a critical link between theory and experiment.

In this Letter, we present a systematic investigation of the excitation spectrum in the J_1-J_2 kagome Heisenberg antiferromagnet (KHAF). We leverage our own recent developments in single-mode excited-state tensor-network methods that overcome previous limitations in order to resolve the full spectrum of low-energy excitations directly for the infinite system, meaning at all wave vectors. By controlling J_2, we track the evolution of the spectrum from the $q = 0$ and $\sqrt{3} \times \sqrt{3}$ magnetically ordered phases to the intermediate QSL phase, revealing how the higher-lying continuum is suppressed into the low-energy magnon branches, closing the spin gap at the emergence of U(1) Dirac QSL behavior. By identifying the fundamental characteristics of the KHAF, our work reveals the spectral signatures that will be crucial for the experimental identification of this QSL phase in quantum magnetic materials realizing the KHAF Hamiltonian.

*These authors contributed equally to this work.
†Contact author: bruce.normand@psi.ch
‡Contact author: navyphysics@iphy.ac.cn
§Contact author: txiang@iphy.ac.cn

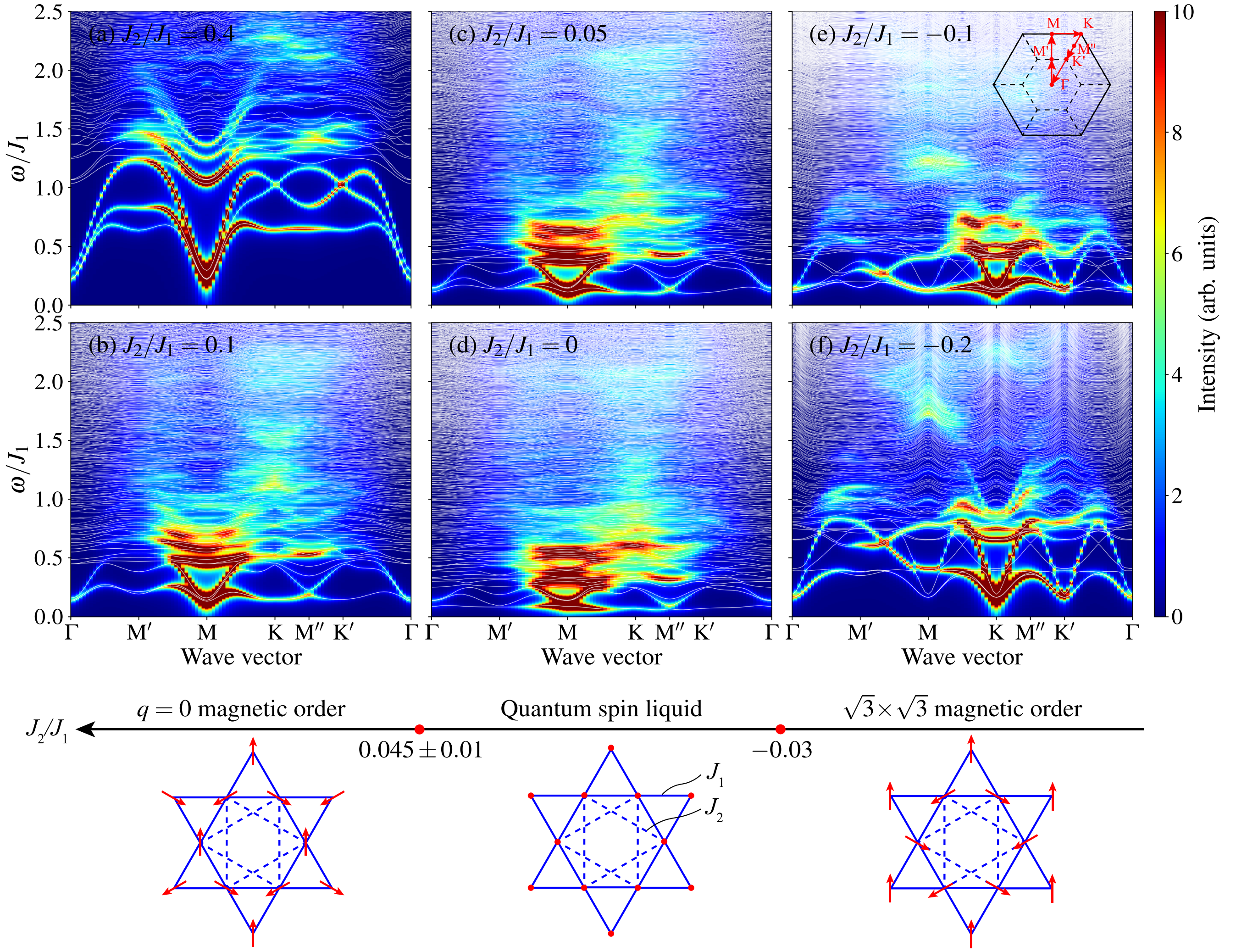

FIG. 1. Spin excitation spectra of the J_1-J_2 kagome Heisenberg antiferromagnet (KHAF). (a)–(f) Example spectra in the $q = 0$ magnetically ordered phase (a),(b), the quantum spin-liquid (QSL) phase (c),(d), and the $\sqrt{3} \times \sqrt{3}$ ordered phase (e),(f). White lines show the energy levels obtained from iPEPS calculations. The inset in panel (e) shows the Brillouin zone and the high-symmetry path followed in our spectra; dashed and solid hexagons mark, respectively, the elementary and extended Brillouin zones. Below the spectra we represent the phase diagram determined by an iPEPS study of the ground states [13].

Theoretically, substantial efforts have been made to understand the ground-state properties of the KHAF by applying the methods of exact diagonalization [4,8,15–17], the density-matrix renormalization group (DMRG) [6,7,9,14,18–22], variational Monte Carlo [11,23–28], and tensor networks [13,29,30]. These studies have uncovered a multiplicity of candidate QSL phases, including gapped, nonchiral $\mathbb{Z}_2$ spin liquids [6,9,18–21,31], chiral spin liquids (CSLs) [9,14,22], and gapless QSLs related to the U(1) Dirac spin liquid (DSL) [7,11,13,14,23–25,27,29,30]. This diversity underlines the sensitivity of KHAF physics and indicates that a definitive characterization will require working beyond the ground state. Numerical studies to date have examined the excitation spectrum of finite-sized systems [8,14,16,28,32–34], with results highly dependent on system size and boundary conditions. Efforts to benchmark the spectrum from experiment remain complicated by the fact that no materials yet available provide a faithful representation of the KHAF, and we summarize this situation in the End Matter. A high-precision calculation of the spectral function in the infinite system is therefore required to clarify the nature of the kagome QSL.

Model and method—We consider the model

$$H = J_1 \sum_{\langle ij \rangle} \vec{S}_i \cdot \vec{S}_j + J_2 \sum_{\langle\langle ij \rangle\rangle} \vec{S}_i \cdot \vec{S}_j \qquad (1)$$

on the kagome lattice with nearest- (J_1) and next-neighbor (J_2) Heisenberg interactions. A tensor-network study of the ground state [13] found a continuous transition from the "$q = 0$" ordered phase [Fig. 1] to a gapless QSL at $J_2/J_1 = 0.045 \pm 0.01$ and a discontinuous transition into the

"$\sqrt{3}\times\sqrt{3}$" ordered phase at $J_2/J_1 = -0.03$. Tensor-network methods operate directly in the limit of infinite system size, which is a major advantage in capturing the key quantum fluctuation effects, and we stress that strikingly different phase boundaries are estimated by techniques restricted to finite systems [10–12,14,34].

The single-mode excitation Ansatz for computing the spectral function [35–37] within the framework of infinite projected entangled-pair states (iPEPS) is summarized in Sec. S1 of the Supplemental Material (SM) [38]. Ground-state optimization and excited-state calculations are performed using automatic differentiation (AD) [45–47]. This method obtains excited states with definite momentum (k) directly, eliminating the spatiotemporal Fourier transforms required in real-time evolution approaches, and thereby yielding excitation spectra with significantly higher resolution. The quantities we calculate are the equal-time spin structure factor,

$$S(\mathbf{k}) = \sum_{\alpha} S^{\alpha\alpha}(\mathbf{k}) \quad \text{with} \quad S^{\alpha\beta}(\mathbf{k}) = \langle 0|S^{\alpha}_{-\mathbf{k}} S^{\beta}_{\mathbf{k}}|0\rangle, \qquad (2)$$

where $\alpha, \beta = x, y, z$, and the spin excitation spectrum,

$$S(\mathbf{k},\omega) = \sum_{\alpha} S^{\alpha\alpha}(\mathbf{k},\omega) \quad \text{with} \qquad (3)$$

$$S^{\alpha\beta}(\mathbf{k},\omega) = \langle 0|S^{\alpha}_{-\mathbf{k}}\delta(\omega - H + E_0)S^{\beta}_{\mathbf{k}}|0\rangle. \qquad (4)$$

The discrete energy levels we obtain are shown by the white lines in Fig. 1 and in postprocessing our data we apply a Lorentzian broadening factor, η, for display purposes, as well as to model an experimental spectral function measured with finite energy resolution.

For the present work, we have developed a number of methodological improvements that speed up our calculations by over 2 orders of magnitude. As described in Sec. S2 of the SM [38], by the reuse of CTMRG projectors [46–48] we achieve efficient parallelization, which we accelerate further by introducing a new fixed-point CTMRG method. This progress allows us to implement systematic spectral-function calculations over the entire Brillouin zone and over a wide range of J_2/J_1. The iPEPS truncation parameter is the tensor bond dimension, D, and finite-D calculations always return a gapped spectrum, from which the intrinsic physics is deduced by extrapolation [13]. Our present calculations allow us to benchmark gapped spectra at fixed D by comparing different J_2 values (below). At fixed J_2, we show a systematic comparison of finite-D spectra in Sec. S3 of the SM [38]. In Sec. S4 [38] we demonstrate that the broadening η cannot close gaps or shift spectral weight, but acts only to round the spectral features. In the figures to follow we use $D = 4$ and $\eta = 0.02J_1$ unless otherwise stated.

Results—Figure 1 illustrates the evolution of the spin excitation spectrum across the J_2/J_1 phase diagram

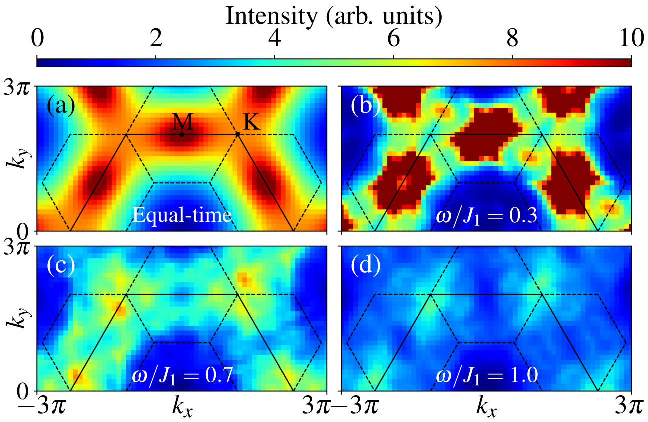

FIG. 2. Spin structure factor of the KHAF at $J_2 = 0$. (a) Equal-time structure factor shown over the entire Brillouin zone. (b)–(d) Dynamic structure factors shown for $\omega = 0.3J_1$ (b), $0.7J_1$ (c), and $1.0J_1$ (d).

(spectra for more J_2 values are shown in Sec. S5 of the SM [38]). Deep in the $q = 0$ ordered phase [$J_2 = 0.4$, Fig. 1(a)] we observe three spin-wave branches with a band width of order J_1, the lowest (the Goldstone mode) having a finite-D gap at the M point. As J_2 is decreased toward the QSL regime [$J_2 = 0.1$, Fig. 1(b)], the three branches not only exhibit a strongly downward energetic renormalization but the dense manifold of higher-lying states begins to cross the third branch. The lowest branch forms an almost flat band along K-K′ and we remark on the persistence of the symmetry-protected crossings between the second and third spin-wave branches (also referred to as Dirac magnons [49]) at the K and K′ points. The ability to resolve these crossings, which are a consequence of reflection and time-reversal symmetries, highlights the accuracy of our tensor-network methods.

At the onset of the QSL [$J_2 = 0.05$, Fig. 1(c)], the spectrum continues its net downward shift and the dense level manifold has fully dispersed spectral weight, which is characteristic of a continuum. As this continuum merges with the upper edge of the low-energy branches, we observe that the minimum of the second-lowest branch approaches the lowest (flat) branch at the M″ point. This behavior is qualitatively different from spin-wave theory, in which the second branch approaches the third, merging with it at $J_2 = 0$ (Sec. S7 of the SM [38]).

The same trends continue at the nearest-neighbor kagome point [$J_2 = 0$, Fig. 1(d)], with the continuum descending below $\omega \approx 0.25J_1$ at all wave vectors and the lowest branch becoming flat at an energy, $\omega < 0.1J_1$, below our finite-D gap, which we benchmark below. A small negative J_2 compresses the spectrum yet more (Fig. S7 of the SM [38]), but further reduction of J_2 drives a first-order transition into the $\sqrt{3}\times\sqrt{3}$ ordered phase [13]. This causes a rapid reemergence of sharp spin-wave excitations [Fig. 1(e)], with the Goldstone mode appearing at K rather than M, and a rapid recovery of their renormalized energy scale toward J_1 [Fig. 1(f)].

Before proceeding to a quantitative analysis of the low-energy spectrum, in Fig. 2 we characterize the spectral function of the QSL throughout the Brillouin zone by showing equal-time and dynamic structure factors at constant energy for $J_2 = 0$. The equal-time structure factor [Fig. 2(a)] has maximal weight at the M point, but strong diffuse intensity spreads along the entire Brillouin-zone boundary. This behavior is in sharp contrast to the ordered phases, where one finds a single dominant peak, either at M in the $q = 0$ phase or at K in the $\sqrt{3} \times \sqrt{3}$ phase; for completeness we show the equal-time structure factor around the high-symmetry path in Sec. S1 of the SM [38] and for a wide range of J_2 values in Sec. S6.

Turning to the dynamic structure factor, at low energies the spectral weight covers an extended but well bounded region around M [Fig. 2(b)]. At energies above the lowest branches, the weight becomes nearly uniform and continuous around the Brillouin-zone boundary [Fig. 2(c)]. While this result is reminiscent of some experimental observations [50,51], moving to still higher energies [Fig. 2(d)] concentrates spectral weight at K, which may be a signature useful for future measurements.

The gapped or gapless nature of the QSL in the KHAF remains under intense debate. To determine its intrinsic nature from finite-D spectral data, we first perform a bond-dimension analysis of the gap for the $J_2 = 0$ case, shown in Fig. 3(a). The gaps at M and M′ (with M″ symmetry-equivalent to M′) decrease as D is increased, following $\Delta \propto 1/D$ within the error bars, which indicates that the QSL is indeed gapless in the large-D limit. By contrast, the energy at K increases with D, and in Fig. 3(a) we apply a linear extrapolation to obtain an upper bound on the width of the lowest band.

As an alternative benchmarking approach, in Fig. 3(b) we analyze the evolution of Δ_{M} and $\Delta_{\mathrm{M}'}$ as functions of J_2. At $J_2/J_1 > 0.05$, in the $q = 0$ phase, the system has a gapless Goldstone mode at M as SU(2) spin symmetry is broken (this mode has finite energy at M′ and M″). Hence the entire blue (Δ_{M}) line in Fig. 3(b) is a finite-D gap. The fact that Δ_{M} takes its smallest values for $J_2/J_1 < 0.05$ indicates that the QSL is indeed gapless, and we take this Δ_{M} value as the criterion defining gap closure. Beyond Fig. 3(a), the fact that the M′-point gap falls below the finite-D gap (Δ_{M}) near $J_2/J_1 \approx 0.05$ in Fig. 3(b) is another criterion for concluding that the M-, M′-, and M″-point gaps all vanish simultaneously upon entering the QSL. The lowest excitation going to zero simultaneously at the M, M′, and M″ points is a primary hallmark of the U(1) DSL [23,26,27] and of crystal momentum fractionalization [26]. The equal-time structure factor of Fig. 2(a) also matches projected-wave-function results obtained for the U(1) DSL [26,27], but is incompatible with alternatives including a gapped QSL and a spinon Fermi-surface QSL.

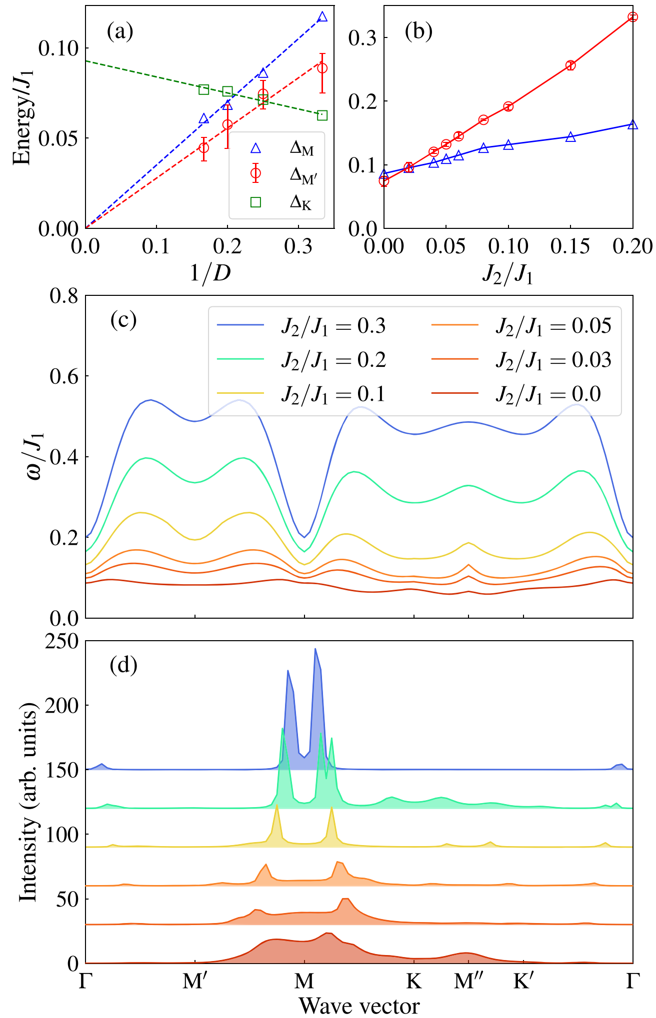

FIG. 3. Properties of the low-energy spectrum. (a) Energy gaps at the M, M′, and K points in the $J_2 = 0$ KHAF shown as functions of $1/D$. Error bars for $\Delta_{\mathrm{M}'}$ represent the variation between M′ points (the Ansatz does not preserve the C_3 symmetry making these equivalent). Dashed lines are guides to the eye. (b) Energy gaps at M and M′ computed as functions of J_2 with $D = 4$. (c) Lowest excitation energy calculated around the high-symmetry path in the Brillouin zone for a range of J_2 values with $D = 4$. (d) Spin excitation spectra at fixed energy $\omega = 0.3J_1$ shown on the same path for the same J_2 and D values.

In Fig. 3(c) we show the dispersion of the lowest excitation branch for a sequence of decreasing J_2 values. The band width is suppressed continuously until at $J_2 = 0$ we find an essentially flat band at the finite-D gap. The emergence around $J_2/J_1 = 0.05$ of a cusp at M″ is a finite-D effect, with M″ becoming the local minimum at higher D (Fig. S4 of the SM [38]). In Fig. 3(d) we show that the constant-energy spectrum at $\omega = 0.3J_1$ has two sharp spin-wave peaks near M when the system is well in the $q = 0$ ordered phase. As J_2 is decreased, the peak intensities are suppressed systematically, while the spectral weight at the M point itself grows, until a broad feature centered at M emerges as the signature of the QSL.

Discussion—The key to a meaningful analysis of QSL properties based on numerical data is achieving a quantitative definition of the terms "gap" and "continuum." Previous studies of ordered magnetic states by the single-mode iPEPS Ansatz [37,46,52–55] demonstrated that the finite-D gap falls systematically with increasing D, restoring the gapless Goldstone mode. With this insight, our ability to scan D over a narrow range and J_2 over a wide range allows us to establish a quantitative criterion for both the finite-D gap and the gap $\Delta_{\mathrm{M}'}$, and hence to deduce the gapless and U(1) Dirac nature of the QSL.

Defining a continuum is a more delicate issue. Tensor-network methods are based on gapped systems and always return a spectrum of integer-spin excitations. The claim that this spectrum is only an effective description of a gapless QSL, which has deconfined $\Delta S = 1/2$ excitations (spinons), is a two-part argument. First, the spectral functions in Figs. 1(b)–1(e) show unbroken series of densely packed lines (a spacing below $0.02J_1$, less still at $D = 5$ in Fig. S3 of the SM [38]) at all energies above the lowest three branches. There is no intensity hierarchy of the type expected from two- and higher-magnon continua [46]. Thus these have a clear physical interpretation as the edge of a continuum marking the onset of spinon deconfinement above a finite energy threshold that is both remarkably low [$0.2J_1$ at $J_2/J_1 = -0.02$, Fig. S7(j) of the SM [38]] and remarkably insensitive to the wave vector (presumably as a consequence of the very flat bands appearing in the KHAF problem). Second, these continua must extend to zero energy at the gapless points. Although we cannot observe this, because the entire lowest band lies at or below our finite-D gap [approximately $0.08J_1$; Fig. 1(d)], we have deduced that this band is massless at M, M′, and M″, while retaining a robust dispersion to an upper band edge close to the finite-D gap. Gap closure at these fractions of the Brillouin-zone dimensions cannot be a property of a real $\Delta S = 1$ excitation, and hence we deduce that the low-energy spectrum must have developed into a continuum above the lowest band, as expected for a U(1) DSL.

The most distinctive features of our QSL spectra [Figs. 1(c) and 1(d)] are (i) strong spectral weight at the finite-D gap and (ii) the continuum at all wave vectors above a very low energy threshold. Property (i) is not shared by any fully gapped QSL, or by a Kitaev-type $\mathbb{Z}_2$ QSL [56], where a single Majorana mode is gapless but the spin response is gapped. However, it is a property of the U (1) DSL, whose low-energy physics is governed by four flavors of two-component Dirac fermion coupled to a U(1) gauge field [23]. Property (ii) alone does not help to classify the QSL phase, but does offer a plausibility argument for why wave-vector-resolved measurements may perceive a full gap. The ongoing debate between gapped and gapless QSLs in the KHAF was shaped by early DMRG studies finding a full gap, and we comment on this in the End Matter. A projective symmetry-group (PSG) analysis of mean-field states in the KHAF found only one gapped $\mathbb{Z}_2$ state, classified as $\mathbb{Z}_2[0,\pi]\beta$, whose energy is competitive with the U(1) Dirac QSL (which is its parent state) [57]. However, detailed studies found very few differences between the physical properties of these two states [11,27], including a gapless spin response for the $\mathbb{Z}_2[0,\pi]\beta$ state, raising the possibility that the PSG mean-field classification may not be appropriate for the KHAF problem. Thus one expects that a gapless QSL in the KHAF can only be the U(1) DSL [23,58,59], and this is confirmed by our result for the M, M′, and M″ gaps.

We remark in closing that, by the nature of the tensor-network Ansatz, our results are highly indicative rather than definitive. Our limitations lie in the "finite-size effect" of the bond dimension, D, which we can vary over only a small range (that is nevertheless sufficient to identify the lowest band and to reveal the continuum). We also applied a level-broadening factor, η, for visualization purposes, and verified that it has no effect on the overall spectral-weight distribution. Our advantages for deducing the intrinsic underlying physics lie in the systematic coverage of energy, wave vector, and J_2 that gives a maximum of certainty to our statements. As the key example, varying J_2 allowed us to benchmark the finite-D gap and hence to make a definite statement that the QSL in the KHAF is gapless.

In summary, we have developed state-of-the-art tensor-network methods to investigate the spin excitation spectrum of the kagome Heisenberg model, using the next-neighbor coupling to control the evolution from the $q = 0$ and $\sqrt{3} \times \sqrt{3}$ magnetically ordered phases into the intermediate QSL regime. In the ordered phases, we compute accurate magnon (and multimagnon) branches lying below a near-uniform continuum, which drives strong quantum renormalization far below the predictions of spin-wave theory. In the QSL phase, we quantify the spectral-weight distribution across the Brillouin zone, finding a broad low-energy feature centered at the M point, a uniform intermediate-energy continuum, and high-energy intensity largely around K. By analyzing the evolution of the low-energy spectrum with D and J_2, we identify vanishing gaps at M, M′, and M″ in the QSL phase, indicating a gapless U(1) Dirac spin liquid. Beyond advancing the understanding of kagome QSLs and offering guidance to future experiments on candidate KHAF materials, our results open a wealth of possibilities for the exploration of exotic quantum states through their spectral functions.

Acknowledgments—We thank Junyi Ji, Chun Zhang, Hong-Chen Jiang, and Wei Zhu for helpful discussions. This work was supported by the Strategic Priority Research Program of Chinese Academy of Sciences (Grant No. XDB0500202), the National Key Research and Development Project of China (Grants No. 2024YFA1408604, No. 2021ZD0301800, and No. 2022YFA1403900), the National Natural Science

Foundation of China (Grants No. 12488201, No. 12322403, and No. 12347107), and the Youth Innovation Promotion Association CAS (Grant No. 2021004). The numerical calculations in this work were carried out on the ORISE Supercomputer of the Chinese Academy of Sciences.

Data availability—The data that support the findings of this article are openly available [60].

[1] P. Anderson, Resonating valence bonds: A new kind of insulator?, Mater. Res. Bull. **8**, 153 (1973).

[2] L. Savary and L. Balents, Quantum Spin Liquids: A Review, Rep. Prog. Phys. **80**, 016502 (2016).

[3] Y. Zhou, K. Kanoda, and T.-K. Ng, Quantum spin liquid states, Rev. Mod. Phys. **89**, 025003 (2017).

[4] P. Sindzingre and C. Lhuillier, Low-energy excitations of the Kagomé antiferromagnet and the spin-gap issue, Europhys. Lett. **88**, 27009 (2009).

[5] S. Sachdev, Kagomé- and triangular-lattice Heisenberg antiferromagnets: Ordering from quantum fluctuations and quantum-disordered ground states with unconfined bosonic spinons, Phys. Rev. B **45**, 12377 (1992).

[6] S. Yan, D. A. Huse, and S. R. White, Spin-liquid ground state of the $S = 1/2$ Kagomé Heisenberg antiferromagnet, Science **332**, 1173 (2011).

[7] Y.-C. He, M. P. Zaletel, M. Oshikawa, and F. Pollmann, Signatures of Dirac Cones in a DMRG Study of the Kagomé Heisenberg Model, Phys. Rev. X **7**, 031020 (2017).

[8] A. M. Läuchli, J. Sudan, and R. Moessner, $S = 1/2$ Kagomé Heisenberg antiferromagnet revisited, Phys. Rev. B **100**, 155142 (2019).

[9] S.-s. Gong, W. Zhu, and D. N. Sheng, Emergent chiral spin liquid: Fractional quantum Hall effect in a Kagomé Heisenberg model, Sci. Rep. **4**, 6317 (2014).

[10] R. Suttner, C. Platt, J. Reuther, and R. Thomale, Renormalization group analysis of competing quantum phases in the $J_1 - J_2$ Heisenberg model on the Kagomé lattice, Phys. Rev. B **89**, 020408(R) (2014).

[11] Y. Iqbal, D. Poilblanc, and F. Becca, Spin-$\frac{1}{2}$ Heisenberg $J_1 - J_2$ antiferromagnet on the Kagomé lattice, Phys. Rev. B **91**, 020402(R) (2015).

[12] F. Kolley, S. Depenbrock, I. P. McCulloch, U. Schollwöck, and V. Alba, Phase diagram of the $J_1 - J_2$ Heisenberg model on the Kagomé lattice, Phys. Rev. B **91**, 104418 (2015).

[13] H. J. Liao, Z. Y. Xie, J. Chen, Z. Y. Liu, H. D. Xie, R. Z. Huang, B. Normand, and T. Xiang, Gapless spin-liquid ground state in the $S = 1/2$ Kagomé antiferromagnet, Phys. Rev. Lett. **118**, 137202 (2017).

[14] W. Zhu, S.-s. Gong, and D. N. Sheng, Identifying spinon excitations from dynamic structure factor of spin-1/2 Heisenberg antiferromagnet on the Kagomé lattice, Proc. Natl. Acad. Sci. U.S.A. **116**, 5437 (2019).

[15] H. Nakano and T. Sakai, Numerical-diagonalization study of spin gap issue of the Kagomé lattice Heisenberg antiferromagnet, J. Phys. Soc. Jpn. **80**, 053704 (2011).

[16] A. M. Läuchli, J. Sudan, and E. S. Sørensen, Ground-state energy and spin gap of spin-1/2 Kagomé-Heisenberg antiferromagnetic clusters: Large-scale exact diagonalization results, Phys. Rev. B **83**, 212401 (2011).

[17] P. Prelovšek, M. Gomilšek, T. Arh, and A. Zorko, Dynamical spin correlations of the Kagomé antiferromagnet, Phys. Rev. B **103**, 014431 (2021).

[18] H. C. Jiang, Z. Y. Weng, and D. N. Sheng, Density matrix renormalization group numerical study of the Kagomé antiferromagnet, Phys. Rev. Lett. **101**, 117203 (2008).

[19] S. Depenbrock, I. P. McCulloch, and U. Schollwöck, Nature of the spin-liquid ground state of the $S = 1/2$ Heisenberg model on the Kagomé lattice, Phys. Rev. Lett. **109**, 067201 (2012).

[20] H.-C. Jiang, Z. Wang, and L. Balents, Identifying topological order by entanglement entropy, Nat. Phys. **8**, 902 (2012).

[21] S. Nishimoto, N. Shibata, and C. Hotta, Controlling frustrated liquids and solids with an applied field in a Kagomé Heisenberg antiferromagnet, Nat. Commun. **4**, 2287 (2013).

[22] R.-Y. Sun, H.-K. Jin, H.-H. Tu, and Y. Zhou, Possible chiral spin liquid state in the $s = 1/2$ Kagomé Heisenberg model, npj Quantum Mater. **9**, 1 (2024).

[23] Y. Ran, M. Hermele, P. A. Lee, and X.-G. Wen, Projected-wave-function study of the spin-1/2 Heisenberg model on the Kagomé lattice, Phys. Rev. Lett. **98**, 117205 (2007).

[24] Y. Iqbal, F. Becca, S. Sorella, and D. Poilblanc, Gapless spin-liquid phase in the kagome spin-$\frac{1}{2}$ Heisenberg antiferromagnet, Phys. Rev. B **87**, 060405(R) (2013).

[25] Y. Iqbal, D. Poilblanc, and F. Becca, Vanishing spin gap in a competing spin-liquid phase in the kagome Heisenberg antiferromagnet, Phys. Rev. B **89**, 020407(R) (2014).

[26] J.-W. Mei and X.-G. Wen, Fractionalized spin-wave continuum in spin liquid states on the kagome lattice, arXiv:1507.03007.

[27] C. Zhang and T. Li, Variational study of the ground state and spin dynamics of the spin-$\frac{1}{2}$ kagome antiferromagnetic Heisenberg model and its implication for herbertsmithite $ZnCu_3(OH)_6Cl_2$, Phys. Rev. B **102**, 195106 (2020).

[28] F. Ferrari, A. Parola, and F. Becca, Gapless spin liquids in disguise, Phys. Rev. B **103**, 195140 (2021).

[29] S. Jiang, P. Kim, J. H. Han, and Y. Ran, Competing spin liquid phases in the $s = \frac{1}{2}$ Heisenberg model on the kagome lattice, SciPost Phys. **7**, 006 (2019).

[30] S. Jahromi, R. Orus, D. Poilblanc, and F. Mila, Spin-$\frac{1}{2}$ kagome Heisenberg antiferromagnet with strong breathing anisotropy, SciPost Phys. **9**, 092 (2020).

[31] J.-W. Mei, J.-Y. Chen, H. He, and X.-G. Wen, Gapped spin liquid with $\mathbb{Z}_2$ topological order for the kagome Heisenberg model, Phys. Rev. B **95**, 235107 (2017).

[32] A. Läuchli and C. Lhuillier, Dynamical Correlations of the Kagome $s = 1/2$ Heisenberg Quantum Antiferromagnet, arXiv:0901.1065.

[33] H. Endo, C. Hotta, and A. Shimizu, From linear to nonlinear responses of thermal pure quantum states, Phys. Rev. Lett. **121**, 220601 (2018).

[34] S. Jiang, A. C. Campello, W. He, J. Wen, D. M. Pajerowski, Y. S. Lee, and H.-C. Jiang, Quantifying the phase diagram

and Hamiltonian of $S = 1/2$ kagome antiferromagnets: Bridging theory and experiment, npj Comput. Mater. **12**, 91 (2026).

[35] S. Östlund and S. Rommer, Thermodynamic limit of density matrix renormalization, Phys. Rev. Lett. **75**, 3537 (1995).

[36] J. Haegeman, B. Pirvu, D. J. Weir, J. I. Cirac, T. J. Osborne, H. Verschelde, and F. Verstraete, Variational matrix product ansatz for dispersion relations, Phys. Rev. B **85**, 100408(R) (2012).

[37] L. Vanderstraeten, M. Mariën, F. Verstraete, and J. Haegeman, Excitations and the tangent space of projected entangled-pair states, Phys. Rev. B **92**, 201111(R) (2015).

[38] See Supplemental Material at http://link.aps.org/supplemental/10.1103/fjjf-xspp, which includes Refs. [39–44], for detailed discussions of (i) the single-mode Ansatz for computing excitation spectra, (ii) the technical developments we implemented to improve these calculations, (iii) a benchmarking of the evolution of the spectrum with the bond dimension D, (iv) an illustration of the effects of η, (v) the evolution of the spectrum with J_2, (vi) the evolution of the static structure factor with J_2, and (vii) the way we performed our linear spin-wave calculations for comparison with the tensor-network spectral function.

[39] P. Corboz, T. M. Rice, and M. Troyer, Competing states in the t-J model: Uniform d-wave state versus stripe state, Phys. Rev. Lett. **113**, 046402 (2014).

[40] K. Wang, S. Feng, P. Zhu, R. Chi, H.-J. Liao, N. Trivedi, and T. Xiang, Fractionalization signatures in the dynamics of quantum spin liquids, Phys. Rev. B **111**, L100402 (2025).

[41] B. Dalla Piazza, M. Mourigal, N. B. Christensen, G. J. Nilsen, P. Tregenna-Piggott, T. G. Perring, M. Enderle, D. F. McMorrow, D. A. Ivanov, and H. M. Rønnow, Fractional excitations in the square-lattice quantum antiferromagnet, Nat. Phys. **11**, 62 (2015).

[42] N. E. Shaik, E. Fogh, B. Dalla Piazza, B. Normand, D. A. Ivanov, and H. M. Rønnow, Confined and deconfined spinon excitations in the rectangular-lattice quantum antiferromagnet, Phys. Rev. B **112**, L020410 (2025).

[43] J. H. P. Colpa, Diagonalization of the quadratic boson Hamiltonian, Physica (Amsterdam) **93A**, 327 (1978).

[44] A. B. Harris, C. Kallin, and A. J. Berlinsky, Possible Néel orderings of the kagomé antiferromagnet, Phys. Rev. B **45**, 2899 (1992).

[45] H.-J. Liao, J.-G. Liu, L. Wang, and T. Xiang, Differentiable Programming Tensor Networks, Phys. Rev. X **9**, 031041 (2019).

[46] R. Chi, Y. Liu, Y. Wan, H.-J. Liao, and T. Xiang, Spin excitation spectra of anisotropic spin-1/2 triangular lattice Heisenberg antiferromagnets, Phys. Rev. Lett. **129**, 227201 (2022).

[47] B. Ponsioen, F. F. Assaad, and P. Corboz, Automatic differentiation applied to excitations with Projected Entangled Pair States, SciPost Phys. **12**, 6 (2022).

[48] W.-L. Tu, L. Vanderstraeten, N. Schuch, H.-Y. Lee, N. Kawashima, and J.-Y. Chen, Generating function for projected entangled-pair states, PRX Quantum **5**, 010335 (2024).

[49] J. Fransson, A. M. Black-Schaffer, and A. V. Balatsky, Magnon Dirac materials, Phys. Rev. B **94**, 075401 (2016).

[50] T.-H. Han, J. S. Helton, S. Chu, D. G. Nocera, J. A. Rodriguez-Rivera, C. Broholm, and Y. S. Lee, Fractionalized excitations in the spin-liquid state of a kagome-lattice antiferromagnet, Nature (London) **492**, 406 (2012).

[51] A. T. Breidenbach, A. C. Campello, J. Wen, H.-C. Jiang, D. M. Pajerowski, R. W. Smaha, and Y. S. Lee, Identifying universal spin excitations in candidate spin-1/2 kagome quantum spin liquid materials, Nat. Phys. **21**, 1957 (2025).

[52] L. Vanderstraeten, J. Haegeman, and F. Verstraete, Simulating excitation spectra with projected entangled-pair states, Phys. Rev. B **99**, 165121 (2019).

[53] B. Ponsioen and P. Corboz, Excitations with projected entangled pair states using the corner transfer matrix method, Phys. Rev. B **101**, 195109 (2020).

[54] R. Chi, J. Hu, H.-J. Liao, and T. Xiang, Dynamical spectra of spin supersolid states in triangular antiferromagnets, Phys. Rev. B **110**, L180404 (2024).

[55] Y. Xu, J. Hasik, B. Ponsioen, and A. H. Nevidomskyy, Simulating spin dynamics of supersolid states in a quantum Ising magnet, Phys. Rev. B **111**, L060402 (2025).

[56] A. Kitaev, Fault-tolerant quantum computation by anyons, Ann. Phys. (Amsterdam) **303**, 2 (2003).

[57] Y.-M. Lu, Y. Ran, and P. A. Lee, $\mathbb{Z}_2$ spin liquids in the $S = 1/2$ Heisenberg model on the kagome lattice: A projective symmetry-group study of Schwinger fermion mean-field states, Phys. Rev. B **83**, 224413 (2011).

[58] M. Hermele, Y. Ran, P. A. Lee, and X.-G. Wen, Properties of an algebraic spin liquid on the kagome lattice, Phys. Rev. B **77**, 224413 (2008).

[59] X.-Y. Song, C. Wang, A. Vishwanath, and Y.-C. He, Unifying description of competing orders in two-dimensional quantum magnets, Nat. Commun. **10**, 4254 (2019).

[60] J. Hu, Dynamical spectral function of the Kagome quantum spin liquid, Zenodo, 10.5281/zenodo.21319354 (2026).

[61] M. P. Shores, E. A. Nytko, B. M. Bartlett, and D. G. Nocera, A Structurally Perfect $s = 1/2$ Kagomé Antiferromagnet, J. Am. Chem. Soc. **127**, 13462 (2005).

[62] Z. Feng, Z. Li, X. Meng, W. Yi, Y. Wei, J. Zhang, Y.-C. Wang, W. Jiang, Z. Liu, S. Li, F. Liu, J. Luo, S. Li, G.-q. Zheng, Z. Y. Meng, J.-W. Mei, and Y. Shi, Gapped spin-1/2 spinon excitations in a new kagome quantum spin liquid compound $Cu_3Zn(OH)_6FBr$, Chin. Phys. Lett. **34**, 077502 (2017).

[63] Y. Li, B. Pan, S. Li, W. Tong, L. Ling, Z. Yang, J. Wang, Z. Chen, Z. Wu, and Q. Zhang, Gapless quantum spin liquid in the $s = 1/2$ anisotropic kagome antiferromagnet $ZnCu_3(OH)_6SO_4$, New J. Phys. **16**, 093011 (2014).

[64] J. Liu, L. Yuan, X. Li, B. Li, K. Zhao, H. Liao, and Y. Li, Gapless spin liquid behavior in a kagome Heisenberg antiferromagnet with randomly distributed hexagons of alternate bonds, Phys. Rev. B **105**, 024418 (2022).

[65] Z. Zeng, X. Ma, S. Wu, H.-F. Li, Z. Tao, X. Lu, X.-h. Chen, J.-X. Mi, S.-J. Song, G.-H. Cao, G. Che, K. Li, G. Li, H. Luo, Z. Y. Meng, and S. Li, Possible Dirac quantum spin liquid in the kagome quantum antiferromagnet $YCu_3(OH)_6Br_2[Br_x(OH)_{1-x}]$, Phys. Rev. B **105**, L121109 (2022).

[66] G. J. Nilsen, M. A. de. Vries, J. R. Stewart, A. Harrison, and H. M. Rønnow, Low-energy spin dynamics of the $s = 1/2$ kagome system herbertsmithite, J. Phys. Condens. Matter **25**, 106001 (2013).

[67] Z. Zeng, C. Zhou, H. Zhou, L. Han, R. Chi, K. Li, M. Kofu, K. Nakajima, Y. Wei, W. Zhang, D. G. Mazzone, Z. Y. Meng, and S. Li, Spectral evidence for Dirac spinons in a kagome lattice antiferromagnet, Nat. Phys. **20**, 1097 (2024).

[68] A. Zorko, S. Nellutla, J. van Tol, L. C. Brunel, F. Bert, F. Duc, J.-C. Trombe, M. A. de Vries, A. Harrison, and P. Mendels, Dzyaloshinsky-Moriya Anisotropy in the Spin-1/2 Kagome Compound $ZnCu_3(OH)_6Cl_2$, Phys. Rev. Lett. **101**, 026405 (2008).

[69] H. O. Jeschke, F. Salvat-Pujol, and R. Valentí, First-principles determination of Heisenberg Hamiltonian parameters for the spin-1/2 kagome antiferromagnet $ZnCu_3(OH)_6Cl_2$, Phys. Rev. B **88**, 075106 (2013).

[70] I. Rousochatzakis, S. R. Manmana, A. M. Läuchli, B. Normand, and F. Mila, Dzyaloshinskii-Moriya anisotropy and nonmagnetic impurities in the $s = \frac{1}{2}$ kagome system $ZnCu_3(OH)_6Cl_2$, Phys. Rev. B **79**, 214415 (2009).

End Matter

Experiment—Several $S = 1/2$ antiferromagnets with kagome geometry have been synthesized, including $\mathrm{ZnCu_3(OH)_6Cl_2}$ (herbertsmithite) [61], $\mathrm{Cu_3Zn(OH)_6FBr}$ (Zn-barlowite) [62], $\mathrm{ZnCu_3(OH)_6SO_4}$ (Zn-brochantite) [63], and $\mathrm{YCu_3(OH)_{6.5}Br_{2.5}}$ (YCOB) [64,65]. INS measurements on some of these materials [50,51,66,67] have found broad excitation continua, which are a generic hallmark of fractionalized excitations. However, an interpretation is complicated by the prevalence of ionic site disorder in most of these systems, which can obscure or mimic the signatures of fractionalization. Further, Cu^{2+} ions in a triangular geometry have unavoidable Dzyaloshinskii-Moriya (DM) interactions [68], as well as possible further-neighbor Heisenberg interactions [69]. Both terms act to stabilize magnetically ordered states, most notably the coplanar $q = 0$ and $\sqrt{3} \times \sqrt{3}$ ordering patterns [13,70], and to modify the spectrum accessible to INS.

Experimental efforts over the past decade have focused on eliminating site disorder [65] and reducing the DM term [62]. A recent study of Zn-barlowite favored the interpretation as a gapped QSL [51] applied to early studies of herbertsmithite [50]. By contrast, further recent work on a YCOB derivative with counter-ion site disorder reported the observation of Dirac cones, and hence of a gapless QSL, albeit with the cones appearing at the K′ points [67]. Given the persisting discrepancies between the paradigm model and the spin Hamiltonians of these materials, we do not attempt to use our spectral functions for modeling purposes, but contribute instead by offering a deeper understanding of the intrinsic spin dynamics of the J_1-J_2 KHAF in both its ordered and QSL phases as a guide for future materials discovery and INS experiment.

DMRG comparison—Early evidence in favor of a gapped QSL in the KHAF with only nearest-neighbor interactions came from DMRG results obtained for relatively narrow cylinders [6,9,18–21]. More recent DMRG studies are divided among the scenarios of the fully gapped $\mathbb{Z}_2$ QSL [31], the gapped CSL [22], and a gapless (Dirac-cone) spinon spectrum [7,14]. Because DMRG, like tensor-network approaches, is based on matrix-product states, both methods share the weakness noted in the main text that a gapped spectrum is an intrinsic feature and the challenge is to deduce the underlying physics from this.

The essential qualitative property of our tensor-network method is that we work on the infinite system, thereby capturing the full two-dimensional reciprocal space with no bias. To the extent that the physics of the U(1) DSL involves optimizing the kinetic energy of nearly-free spinonic quasiparticles, it is eminently possible that the restriction to only few wave vectors around the DMRG cylinder may constitute a strong bias. We draw attention once again to the very different QSL phase boundaries in J_2 obtained in our work [13] and by finite-system methods [12,14,34], which indicate that the two approaches are studying a quite different phase competition. (This may not come as a total surprise, given the extremely delicate nature of the KHAF problem). We assert that any results obtained for the infinite system have an intrinsic advantage and justify this statement from the accuracy of the spectral functions we obtained at all energies in the $q = 0$ ordered phase near the continuous J_2-driven transition to the QSL.